Length-Dependent Modulation of Cytoskeletal Remodeling and Mechanical Energetics in Airway Smooth Muscle

Hak Rim Kim[1,3], Katrina Liu[1], Thomas J. Roberts[2], and Chi-Ming Hai[1]

[1]Department of Molecular Pharmacology, Physiology, and Biotechnology, and [2]Department of Ecology and Evolutionary Biology, Brown University, Providence, Rhode Island; and [3]Department of Pharmacology, College of Medicine, Dankook University, Cheonan-si, Chungnam, Republic of Korea

Actin cytoskeletal remodeling is an important mechanism of airway smooth muscle (ASM) contraction. We tested the hypothesis that mechanical strain modulates the cholinergic receptor–mediated cytoskeletal recruitment of actin-binding and integrin-binding proteins in intact airway smooth muscle, thereby regulating the mechanical energetics of airway smooth muscle. We found that the carbachol-stimulated cytoskeletal recruitment of actin-related protein-3 (Arp3), metavinculin, and talin were up-regulated at short muscle lengths and down-regulated at long muscle lengths, suggesting that the actin cytoskeleton–integrin complex becomes enriched in cross-linked and branched actin filaments in shortened ASM. The mechanical energy output/input ratio during sinusoidal length oscillation was dependent on muscle length, oscillatory amplitude, and cholinergic activation. The enhancing effect of cholinergic stimulation on mechanical energy output/input ratio at short and long muscle lengths may be explained by the length-dependent modulation of cytoskeletal recruitment and crossbridge cycling, respectively. We postulate that ASM functions as a hybrid biomaterial, capable of switching between operating as a cytoskeleton-based mechanical energy store at short muscle lengths to operating as an actomyosin-powered mechanical energy generator at long muscle lengths. This postulate predicts that targeting the signaling molecules involved in cytoskeletal recruitment may provide a novel approach to dilating collapsed airways in obstructive airway disease.

Keywords: airway smooth muscle; asthma; bronchoconstriction; cytoskeleton; mechanics

Actin cytoskeletal remodeling is an important mechanism of airway smooth muscle contraction (1). Airway smooth muscle functions in a mechanically active environment, and undergoes shortening and lengthening during breathing cycles. We and other investigators showed that muscle length is an important determinant of cholinergic receptor–coupled signaling pathways in intact airway smooth muscle, for example, in phosphatidylinositol breakdown, intracellular [Ca^{2+}] regulation, extracellular signal-regulated kinase (Erk1/2) mitogen-activated protein kinase (MAPK) phosphorylation, myosin light chain phosphorylation, paxillin phosphorylation, and focal adhesion kinase phosphorylation (2–7). Several of these signaling pathways (e.g., phosphatidylinositol breakdown and focal adhesion kinase phosphorylation) are known to regulate cytoskeletal remodeling in multiple cell types (8–11). We previously showed that cholinergic receptor activation stimulates the cytoskeletal recruitment of actin-binding and integrin-binding proteins such as α-actinin and talin in intact airway smooth muscle (12). In addition, other studies suggested the involvement of Erk1/2 MAPK in cytoskeletal remodeling in intact airway smooth muscle and cultured vascular smooth muscle cells (12, 13). In this study, we tested the hypothesis that mechanical strain modulates the cholinergic receptor–mediated cytoskeletal recruitment of actin-binding and integrin-binding proteins in intact airway smooth muscle in an Erk1/2 MAPK-dependent manner, thereby regulating mechanical energetics of airway smooth muscle, as shown in the schematic outline:

$$\text{Muscle Length} \rightarrow \text{Erk1/2} \rightarrow \text{Cytoskeletal Recruitment} \rightarrow \text{Mechanical Energetics}$$

To study the length dependencies of mechanical energetics, we measured the mechanical energy output/input ratio during the sinusoidal length oscillation of unstimulated and carbachol-stimulated tissues held at different muscle lengths, and interpreted the data on mechanical energetics in terms of cytoskeletal recruitment and crossbridge activation.

We focused on several cytoskeletal proteins: α-actinin, α-smooth muscle (α-SM) actin, actin-related protein-3 (Arp3), metavinculin, talin, and vinculin, based on the following rationale. α-Actinin is a cross-linker of actin filaments, whereas α-SM actin is the basic subunit of actin filaments. Arp3 is a subunit of the Arp2/3 complex that initiates the branching of actin filaments (14). Metavinculin and vinculin are linker proteins that connect the actin cytoskeleton to integrin receptors via talin. Metavinculin and vinculin are homologous proteins derived from the alternative splicing of a single gene (15, 16). Vinculin is ubiquitous, whereas metavinculin is found only in smooth and cardiac muscle cells (17).

CLINICAL RELEVANCE

The results of this study suggest that the up-regulation of cytoskeletal recruitment in highly shortened airway smooth muscle may be an important mechanism of reduced airway distensibility in asthma. Accordingly, targeting the signaling molecules involved in cytoskeletal recruitment, such as phosphatidylinositol 4,5 bisphosphate and focal adhesion kinase, may provide a novel approach to the treatment of obstructive airway diseases such as asthma.

MATERIALS AND METHODS

Tissue Preparation

Bovine tracheae were collected from a local abattoir and transported to the laboratory in ice-cold (4°C) physiologic salt solution (PSS) of the composition (in mM): 140 NaCl, 4.7 KCl, 1.2 Na_2HPO_4,

(*Received in original form April 2, 2010 and in final form July 11, 2010*)

This study was supported by National Heart, Lung, and Blood Institute grant HL-52714.

Correspondence and requests for reprints should be addressed to Chi-Ming Hai, Ph.D., Department of Molecular Pharmacology, Physiology, and Biotechnology, Brown University, Box G-B3, 171 Meeting Street, Providence, RI 02912. E-mail: Chi-Ming_Hai@brown.edu

This article has an online supplement, which is accessible from this issue's table of contents at www.atsjournals.org

Am J Respir Cell Mol Biol Vol 44. pp 888–897, 2011
Originally Published in Press as DOI: 10.1165/rcmb.2010-0144OC on August 12, 2010
Internet address: www.atsjournals.org

2.0 3-(N-morpholino)propanesulfonic acid (MOPS) (pH 7.4 at 37°C), 0.02 Na_2-EDTA, 1.2 $MgSO_4$, 1.6 $CaCl_2$, and 5.6 D-glucose. The smooth muscle layer was excised from the trachea, as described previously (12). Please see the online supplement for additional details.

Tissue Homogenization, Cytoskeletal Fractionation, SDS-PAGE, and Western Blotting

Our procedure was described previously (12). Briefly, muscle strips were homogenized in a cold (4°C) cytoskeletal extraction buffer containing 20 mM Tris HCl (pH 7.5), 2 mM EDTA, 2 mM EGTA, 6 mM mercaptoethanol, 50 μg/ml aprotinin, 50 μg/ml leupeptin, 0.1 mM Na_3VO_4, 1 mM phenylmethylsulfonyl fluoride, and 50 mM sodium fluoride. Tissue homogenates were centrifuged at 100,000 × *g* in an ultracentrifuge (Beckman, Fullerton, CA) for 1 hour at 4°C. After centrifugation, the supernatant represented the cytosolic fraction, whereas the pellet represented the cytoskeletal/membrane fraction. Several studies showed that the low ionic strength extraction buffer used in this study is effective at extracting cytosolic and cytoskeletal fractions (12, 18–21). We did not separate the pellet further into cytoskeleton and membrane fractions because the cell membrane is an integral component of the membrane–cytoskeleton complex (11, 22, 23). Pellets were homogenized in SDS buffer containing 1% SDS, 10% glycerol, and 20 mM dithiothreitol at 20 mg/ml, as described previously (24). The supernatant was mixed with an equal volume of 2 × SDS buffer. Equal volumes of pellet and supernatant samples from a given muscle strip were boiled for 2 minutes and then loaded into neighboring wells for SDS-PAGE and Western blotting. The pellet/supernatant ratio for each protein was calculated from pellet band density × pellet sample volume/supernatant band density × supernatant sample volume, as described previously (12).

Measurement of Mechanical Energy Output/Input Ratio during Sinusoidal Length Oscillation

The procedure for sinusoidal length oscillation was described previously (25). Briefly, one end of a muscle strip is fixed to a stainless clamp, and the other end of the muscle strip is connected to the lever arm via a stainless steel wire. Muscle strips were oscillated sinusoidally for 36 cycles at 1 Hz, and at amplitudes ranging from 0.1–1% reference length (Lo), using a computer-controlled Dual Mode Lever System (Model 300 B; Aurora Scientific, Inc., Aurora, Ontario, Canada). In muscle length perturbation experiments, a 1% change in muscle length is considered quite large in relation to the crossbridge step size/half-sarcomere length ratio, and when applied rapidly, is expected to induce crossbridge detachment and force transients (26). Data were acquired at 100 Hz, and analyzed using IGOR Pro, version 6.0 (Wavemetrics, Inc., Lake Oswego, OR). We computed mechanical power by multiplying force and velocity (the time differential of length). We then computed the ratio of energy output/input during the last 10 cycles of length oscillation by integrating the power output and power input graphs with time.

RESULTS

Length Dependence of Active Force Development and Cytoskeletal Recruitment of Actin-Binding and Integrin-Binding Proteins

In these experiments, equilibrated muscle strips held at 0.3, 0.7, or 1.0 Lo were either unstimulated or stimulated by 1 μM carbachol for 30 minutes As shown in Table 1, active forces developed by carbachol-stimulated muscle strips were higher than the corresponding basal forces developed by unstimulated muscle strips at 0.7 and 1.0 Lo, but not at 0.3 Lo. Unstimulated and carbachol-stimulated muscle strips held at 0.3, 0.7, or 1.0 Lo were then homogenized for cytoskeletal fractionation, SDS-PAGE, and Western blotting.

α-SM actin and Arp3. For α-SM actin, as shown in Figure 1A (*first* and *second rows* of *immunoblot*), band densities were higher in the pellet than in the supernatant, and were relatively independent of muscle length and carbachol stimulation, consistent with the values of pellet/supernatant ratios shown in Figure 1C (*circles*). Two-way ANOVA indicated that neither 1 μM carbachol nor muscle length exerted a significant effect on the pellet/supernatant ratio of α-SM actin.

TABLE 1. LENGTH DEPENDENCIES OF ACTIVE FORCE DEVELOPMENT BY UNSTIMULATED, CARBACHOL-STIMULATED, AND U0126-TREATED, CARBACHOL-STIMULATED MUSCLE STRIPS

	Active Force (Fraction of Fo; Means ± SEM; n = 7–9)		
Muscle Length	Unstimulated	Carbachol	U0126 + Carbachol
0.3 Lo	0.00 ± 0.00	0.020 ± 0.005	0.004 ± 0.003
0.7 Lo	0.00 ± 0.00	0.65 ± 0.04*	0.60 ± 0.07*
1.0 Lo	0.14 ± 0.04	0.98 ± 0.04*	1.01 ± 0.05*

Length is expressed as fraction of reference length (Lo). Active force is expressed as fraction of active force (Fo) stimulated by K^+-depolarization.

* Significantly different from basal force in unstimulated muscle strips ($P < 0.05$).

As a validation of the cytoskeletal fractionation method, Figure 1B (*immunoblot*, *second row*) shows that the actin filament–associated protein, caldesmon, is localized exclusively in the pellet fraction, whereas α-SM actin is localized in both pellet and supernatant fractions (Figure 1B, *immunoblot*, *first row*). Caldesmon is a major actin-binding and calmodulin-binding protein of smooth muscle. General consensus exists that caldesmon remains attached to the actin filament throughout the contraction–relaxation cycle in smooth muscle (27). Therefore, caldesmon is a useful marker of actin filaments in smooth muscle. The observed presence of caldesmon in the pellet fraction and the absence of caldesmon in the supernatant fraction (Figure 1B) indicate that the actin cytoskeleton is extracted in the pellet fraction.

In preliminary experiments, we determined the optimal loading volumes for detecting individual cytoskeletal proteins by Western blotting. For example, the loading volume for detecting α-SM actin was only 25% of the loading volume for detecting Arp3. In addition, the calculation of the pellet/supernatant ratio for each cytoskeletal protein in each tissue sample was based on (pellet band density × pellet volume)/(supernatant band density × supernatant volume). Therefore, small variations in loading between samples are accounted for by the pellet and supernatant volumes in the calculation. Care was also taken to expose films below saturation for all bands. As shown in Figure 1D, the pellet/supernatant ratios for α-SM actin from nine samples of carbachol-stimulated tissues held at Lo were relatively independent of the film densities of the pellet bands recorded from these samples.

For Arp3, as shown in Figure 1A (*third* and *fourth rows* of *immunoblot*), the band density was higher in the pellet than in the supernatant in carbachol-stimulated muscle strips held at 0.3 Lo, but not in other experimental conditions, consistent with the values of pellet/supernatant ratios shown in Figure 1C (*squares*). Band densities were generally higher for α-SM actin than for Arp3, because α-SM actin is a more abundant protein. As shown in Figure 1C (*solid squares*), the pellet/supernatant ratios of Arp3 in carbachol-stimulated muscle strips held at 0.3, 0.7, and 1.0 Lo were (means ± SEM): 2.18 ± 0.39, 1.41 ± 0.26, and 1.04 ± 0.14, respectively. The Arp3 pellet/supernatant ratio was significantly higher in carbachol-stimulated than unstimulated muscle strips at 0.3 Lo, but not at 0.7 and 1.0 Lo. Two-way ANOVA indicated that both 1 μM carbachol and muscle length exerted significant effects on the pellet/supernatant ratio of Arp3.

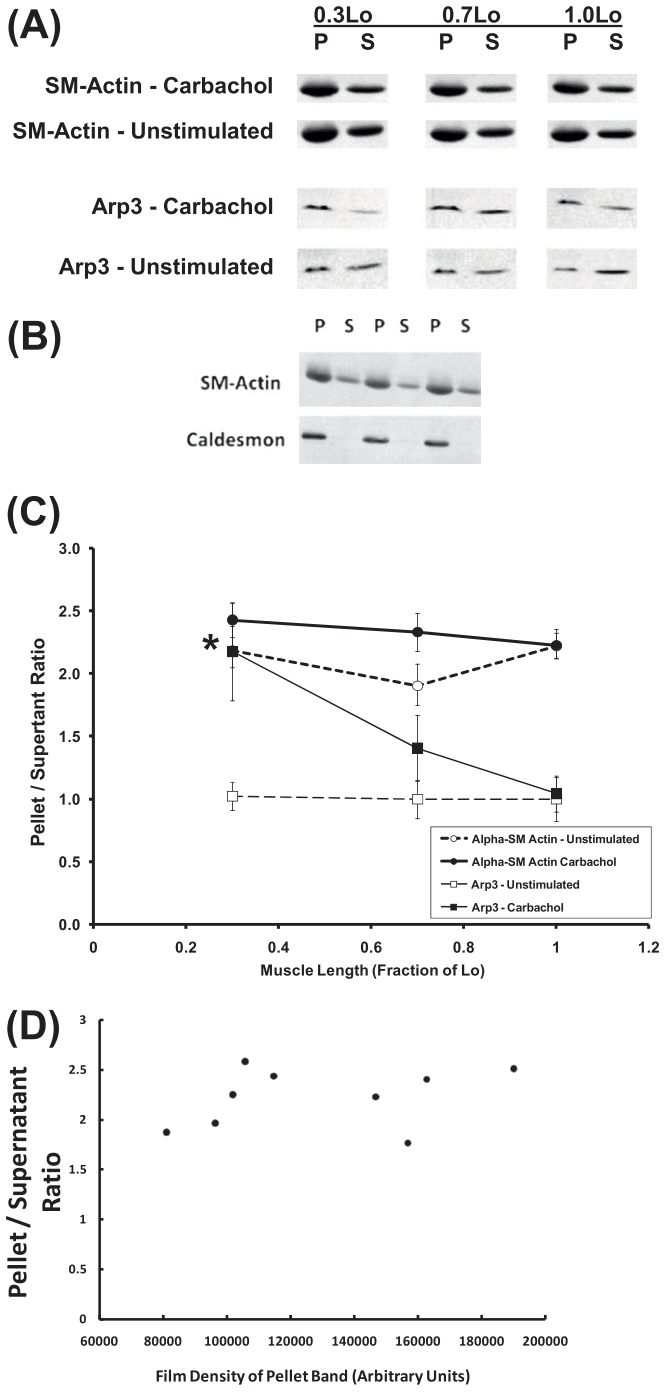

Figure 1. (*A*) Immunoblots of α-smooth muscle (α-SM) actin and actin-related protein-3 (Arp3) in pellet (P) and supernatant (S) fractions extracted from unstimulated and carbachol-stimulated tissues. (*B*) Caldesmon, a filamentous actin–associated protein, is localized exclusively in the P fraction, whereas α-SM actin is localized in both P and S fractions. Three independent samples are shown. (*C*) Length dependencies of P/S ratios of α-SM actin (*circles*) and Arp3 (*squares*) in unstimulated (*open symbols*) and carbachol-stimulated (*solid symbols*) tissues. Data are presented as means ± SEM ($n = 9$). *Significantly different from basal P/S in unstimulated tissues held at the same muscle length ($P < 0.05$). (*D*) P/S ratios for α-SM actin were relatively independent of the film densities of pellet bands recorded in these samples. The nine samples shown here were taken from carbachol-stimulated tissues held at reference length (Lo).

Metavinculin and vinculin. As shown in Figure 2A (*immunoblot*), metavinculin and vinculin appeared as two bands of different molecular weights. The pellet/supernatant band density ratios for metavinculin and vinculin were slightly higher at 0.3 Lo than at other lengths, in general agreement with the values of pellet/supernatant ratios shown in Figure 2A. In this example, the calculated pellet/supernatant ratios were slightly higher than the relative band densities in the pellet and supernatant, because pellet volumes were slightly higher than supernatant volumes in this experiment. As shown in Figure 2A (*solid circles*), the pellet/supernatant ratios of metavinculin in carbachol-stimulated muscle strips held at 0.3, 0.7, and 1.0 Lo were 1.28 ± 0.07, 1.09 ± 0.07, and 1.00 ± 0.06, respectively, which were significantly higher than the corresponding values in unstimulated muscle strips held at 0.3 and 0.7 Lo, but not at 1.0 Lo. As shown in Figure 2A (*solid squares*), the pellet/supernatant ratios of vinculin in carbachol-stimulated muscle strips held at 0.3, 0.7, and 1.0 Lo were 0.92 ± 0.05, 0.79 ± 0.06, and 0.74 ± 0.06, respectively, which were significantly higher than the corresponding values in unstimulated muscle strips held at 0.3 and 0.7 Lo, but not at 1.0 Lo. Two-way ANOVA indicated that both 1 μM carbachol and muscle length exerted significant effects on the pellet/supernatant ratio of metavinculin (Figure 2A). In contrast, two-way ANOVA indicated that 1 μM carbachol, but not muscle length, exerted a significant effect on the pellet/supernatant ratio of vinculin.

Talin and α-actinin. As shown in Figure 2B (*first* and *second rows* of *immunoblot*), talin appeared as two bands of different molecular weights. The calpain-mediated proteolysis of talin into head (∼ 50 kD) and rod (∼190 kD) fragments (which may have occurred within the focal adhesion/dense plaque) is known to regulate the binding of talin to integrin (28–30). In this study, the anti-talin monoclonal antibody (clone 8 d4; Sigma, St. Louis, MO) recognized an epitope in the rod fragment, and was therefore expected to label the two talin bands corresponding to intact talin and the rod fragment (Figure 2B). Because the talin rod fragment represents a minor fraction of total talin (Figure 2B), and the cell biology of talin proteolysis is not fully understood, we calculated pellet/supernatant ratios for talin by summing the two bands of talin for both the pellet and supernatant.

As shown in Figure 2B (*first* and *second rows* of *immunoblot*), the band density of talin was generally higher in the pellet than in the supernatant, and the pellet/supernatant band density ratio was higher at 0.3 Lo than at other lengths, consistent with the values of pellet/supernatant ratios shown in Figure 2B (*circles*). As shown in Figure 2B (*solid circles*), the pellet/supernatant ratios of talin in carbachol-stimulated muscle strips held at 0.3, 0.7, and 1.0 Lo were 6.87 ± 1.39, 3.35 ± 0.26, and 3.14 ± 0.45, respectively, which were not significantly different from the corresponding values in unstimulated muscle strips. Two-way ANOVA indicated that both 1 μM carbachol and muscle length exerted significant effects on the pellet/supernatant ratio of talin (Figure 2B).

For α-actinin, as shown in Figure 2B (*third* and *fourth rows* of *immunoblot*), the band density was generally higher in the pellet than in the supernatant, and the pellet/supernatant band density ratio was higher in carbachol-stimulated than unstimulated tissues, consistent with the values of pellet/supernatant ratios shown in Figure 2B (*squares*). As shown in Figure 2B (*solid squares*), the pellet/supernatant ratios of α-actinin in carbachol-stimulated muscle strips held at 0.3, 0.7, and 1.0 Lo were 2.67 ± 0.45, 2.18 ± 0.35, and 1.70 ± 0.25, respectively, which were significantly higher than the corresponding values in unstimulated muscle strips. Two-way ANOVA indicated that 1 μM carbachol, but not muscle length, exerted a significant effect on the pellet/supernatant ratio of α-actinin.

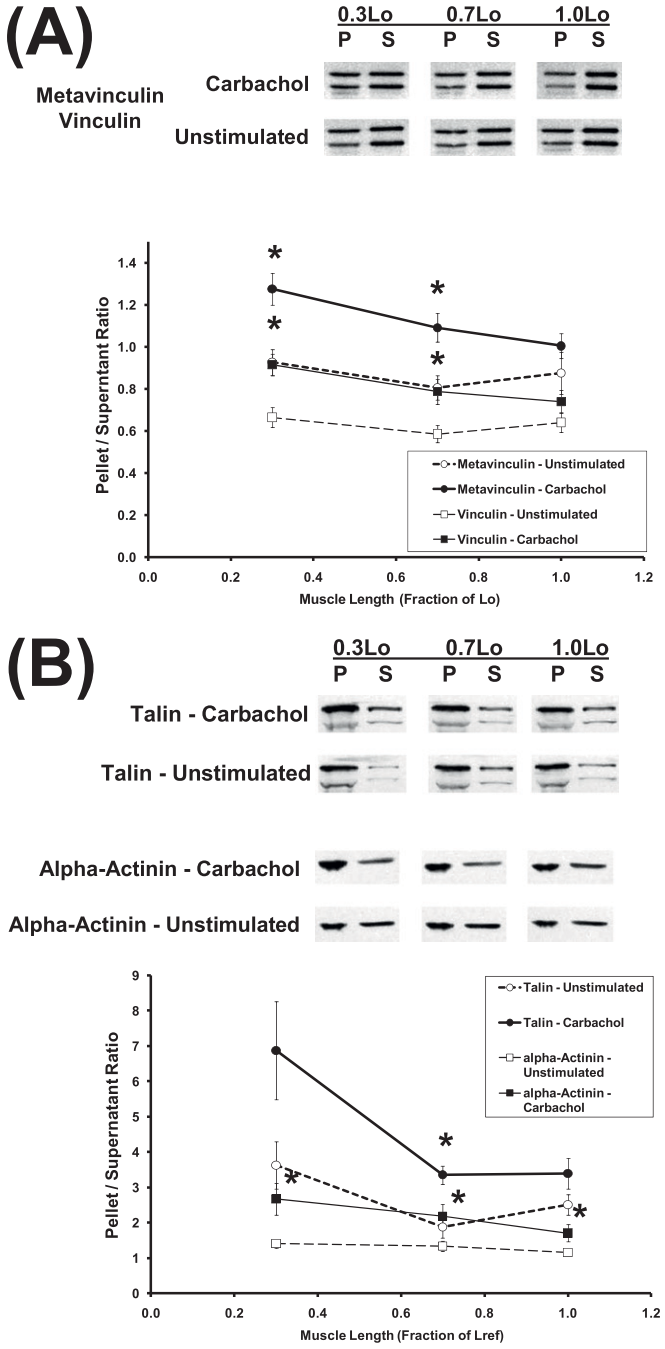

Figure 2. Length dependencies of (*A*) pellet/supernatant ratios of metavinculin (*circles*) and vinculin (*squares*), and (*B*) pellet/supernatant ratios of α-actinin (*squares*) and talin (*circles*) in unstimulated (*open symbols*) and carbachol-stimulated (*solid symbols*) tissues. Data are presented as means ± SEM (n = 8–9). *Significantly different from basal pellet/supernatant in unstimulated tissues held at the same muscle length ($P < 0.05$).

Length Dependencies of Mechanical Energy Output/Input Ratio during Sinusoidal Length Oscillation of Unstimulated and Carbachol-Stimulated Muscle Strips

In these experiments, unstimulated and carbachol-stimulated muscle strips held at 0.3, 0.7, or 1.0 Lo were oscillated sinusoidally at a frequency of 1 Hz and amplitudes ranging from 0.1–1% Lo. This moderately high frequency was chosen to perturb crossbridge cycling, to reveal both crossbridge and non–crossbridge mechanisms in the regulation of mechanical energetics. A similarly high oscillatory frequency was used for measuring the distensibility of the airway system by forced oscillation technique in patients (31). Figures 3 and 4 show typical datasets of mechanical power input and output during the sinusoidal length oscillation of unstimulated and carbachol-stimulated muscle strips held at 0.3, 0.7, and 1.0 Lo, at an amplitude of 1% Lo and a frequency of 1 Hz. In Figures 3 and 4, the *bottom green graph* indicates the mechanical power input imposed upon a muscle strip during the lengthening phase, whereas the *top blue graph* indicates the mechanical power output that was returned by a muscle strip during the shortening phase. A comparison of the ordinates in Figures 3 and 4 indicates that mechanical power input and output both increased with muscle length, that is, lowest at 0.3 Lo, intermediate at 0.7 Lo, and highest at Lo. Furthermore, a comparison of the areas under the power input and power output graphs indicates that the power input was higher than the power output at each of the three muscle lengths, but the relative areas under the power output versus power input graphs appeared to be variable and dependent on muscle length and cholinergic stimulation.

We calculated the ratio of mechanical energy input/output during sinusoidal length oscillation by integrating the power input and power output with time. Figure 5A compares the mechanical energy output/input ratio in unstimulated (*broken lines*) and carbachol-stimulated (*solid lines*) muscle strips as a function of muscle length during sinusoidal length oscillation at 1 Hz, at amplitudes ranging from 0.1–1% Lo. As shown in Figure 5A, the mechanical energy output/input ratio was length-dependent in both unstimulated and carbachol-stimulated muscle strips (lowest at 0.3 Lo, and highest at Lo), oscillatory amplitude–dependent (smallest at 0.1% Lo, and largest at 1% Lo), and activation-dependent (lower in unstimulated muscle strips, and higher in carbachol-stimulated muscle strips). Therefore, we compared the length dependencies of mechanical energy output/input ratios in carbachol-stimulated and unstimulated muscle strips at individual oscillatory amplitudes.

At an oscillatory amplitude of 0.1% Lo, mechanical energy output/input ratios in carbachol-stimulated muscle strips at 0.3, 0.7, and 1.0 Lo were 95.0% ± 0.4%, 98.3% ± 0.1%, and 99.2% ± 0.1%, respectively (Figure 5A, *solid circles*), which were significantly higher than the corresponding ratios (89.7% ± 2.6%, 92.6% ± 1.2%, and 98.3% ± 0.3%, respectively) in unstimulated muscle strips (Figure 5A, *open circles*). At an oscillatory amplitude of 0.5% Lo, the mechanical energy output/input ratios in carbachol-stimulated muscle strips at 0.3, 0.7, and 1.0 Lo were 79.0 ± 2.4%, 92.7 ± 0.6%, and 96.2 ± 0.2%, respectively (Figure 5A, *solid squares*), which were significantly higher than the corresponding ratios (74.6% ± 17.7%, 78.5% ± 5.0%, and 93.0% ± 1.3%, respectively) in unstimulated muscle strips at 0.7 and 1.0 Lo (Figure 5A, *open squares*), but not at 0.3 Lo. At an oscillatory amplitude of 1% Lo, the mechanical energy output/input ratios in carbachol-stimulated muscle strips at 0.3, 0.7, and 1.0 Lo were 57.0% ± 4.9%, 84.2% ± 1.9%, and 91.8% ± 0.4%, respectively (Figure 5A, *solid triangles*), which were significantly higher than the corresponding ratios (35.7% ± 11.2%, 51.0% ± 17.9%, and 86.7% ± 2.8%, respectively) in unstimulated muscle strips (Figure 5A, *open triangles*).

Length Dependence of Erk1/2 MAPK Phosphorylation

We measured Erk1 and Erk2 phosphorylation by Western blotting. For each experiment, values of Erk1 or Erk2 phosphorylation were normalized to the corresponding basal values of Erk1 or Erk2 phosphorylation in unstimulated muscle strips held at Lo. As shown in Figure 5B (*solid circles*), Erk1

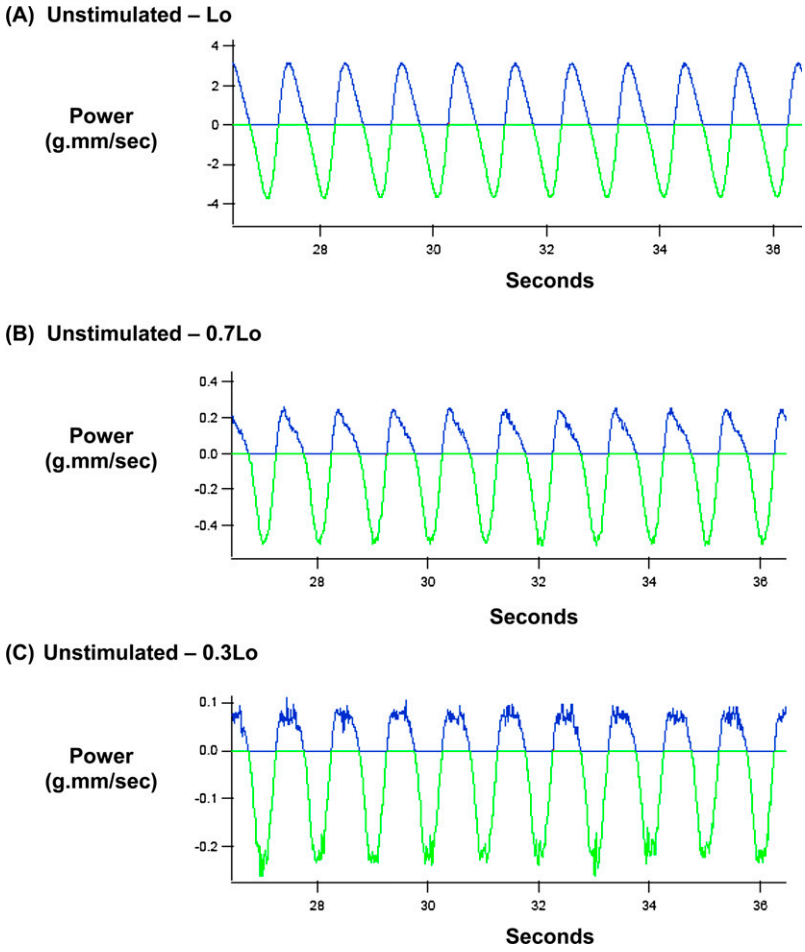

Figure 3. Mechanical power input (*green*) and output (*blue*) during sinusoidal length oscillation of an unstimulated bovine tracheal smooth muscle held at (*A*) Lo, (*B*) 0.7 Lo, and (*C*) 0.3 Lo. In this experiment, oscillatory amplitude and frequency were 1% Lo and 1 Hz, respectively.

phosphorylation in carbachol-stimulated muscle strips at 0.3, 0.7, and 1.0 Lo were 1.61 ± 0.26, 3.01 ± 0.46, and 5.28 ± 0.92, respectively, which were significantly higher than the corresponding values (0.25 ± 0.11, 0.32 ± 0.13, and 1.0, respectively) in unstimulated muscle strips. Similarly, as shown in Figure 5B (*solid squares*), Erk2 phosphorylation in carbachol-stimulated muscle strips at 0.3, 0.7, and 1.0 Lo were 2.56 ± 0.74, 3.73 ± 0.93, and 6.38 ± 1.51, respectively, which were significantly higher than the corresponding values (0.87 ± 0.14, 0.67 ± 0.14, and 1.0, respectively) in unstimulated muscle strips.

Effect of U0126 on Length-Dependent Cytoskeletal Recruitment of Talin and Metavinculin, and Active Force Development in Carbachol-Stimulated Muscle Strips

Next, we tested the hypothesis that length-dependent Erk1/2 MAPK activation mediates the length-dependent cytoskeletal recruitment of talin and metavinculin in 1 μM carbachol-stimulated tissues, using U0126, an inhibitor of Erk1/2 MAPK kinase (MEK1/2). In these experiments, equilibrated muscle strips after K^+-depolarization were allowed to relax for 1 hour in PSS containing 10 μM U0126, and were then either unstimulated or stimulated with 1 μM carbachol in the presence of 10 μM U0126 for 30 minutes.

We focused on talin and metavinculin, because muscle length significantly modulates the cytoskeletal recruitment of these two proteins (Figure 2). As shown in Figure 6A, U0126 had an insignificant effect on the pellet/supernatant ratios of talin at all measured lengths. Consistently, two-way ANOVA indicated that U0126 had an insignificant effect, whereas muscle length had a significant effect, on the pellet/supernatant ratio of talin in 1 μM carbachol-stimulated tissues, with insignificant interaction between U0126 and length in determining the pellet/supernatant ratio of talin. In contrast, as shown in Figure 6B, U0126 significantly increased the pellet/supernatant ratio of metavinculin at Lo, but not at 0.3 or 0.7 Lo. Consistently, two-way ANOVA indicated that both U0126 and muscle length exerted significant effects on the pellet/supernatant ratio of metavinculin, with significant interaction between U0126 and muscle length in determining the pellet/supernatant ratio of metavinculin. These results suggest that Erk1/2 MAPK is involved in the length-dependent modulation of cytoskeletal recruitment of metavinculin, but not talin, in 1 μM carbachol-stimulated tissues.

As shown in Table 1, active forces developed by U0126-treated, carbachol-stimulated muscle strips at 0.3, 0.7, and 1.0 Lo were not significantly different from the corresponding values in untreated carbachol-stimulated muscle strips. We also determined the effect of U0126 on the mechanical energy output/input ratio during sinusoidal length oscillation in carbachol-stimulated muscle strips, similar to the experiments shown in Figure 5A. However, at all amplitudes imposed, 10 μM U0126 exerted no significant effect on the length dependence of mechanical energy input/output ratios in carbachol-stimulated muscle strips (data not shown).

DISCUSSION

Muscle length is an important determinant of the multiple cholinergic receptor–coupled signaling pathways implicated in crossbridge activation and cytoskeletal remodeling in airway

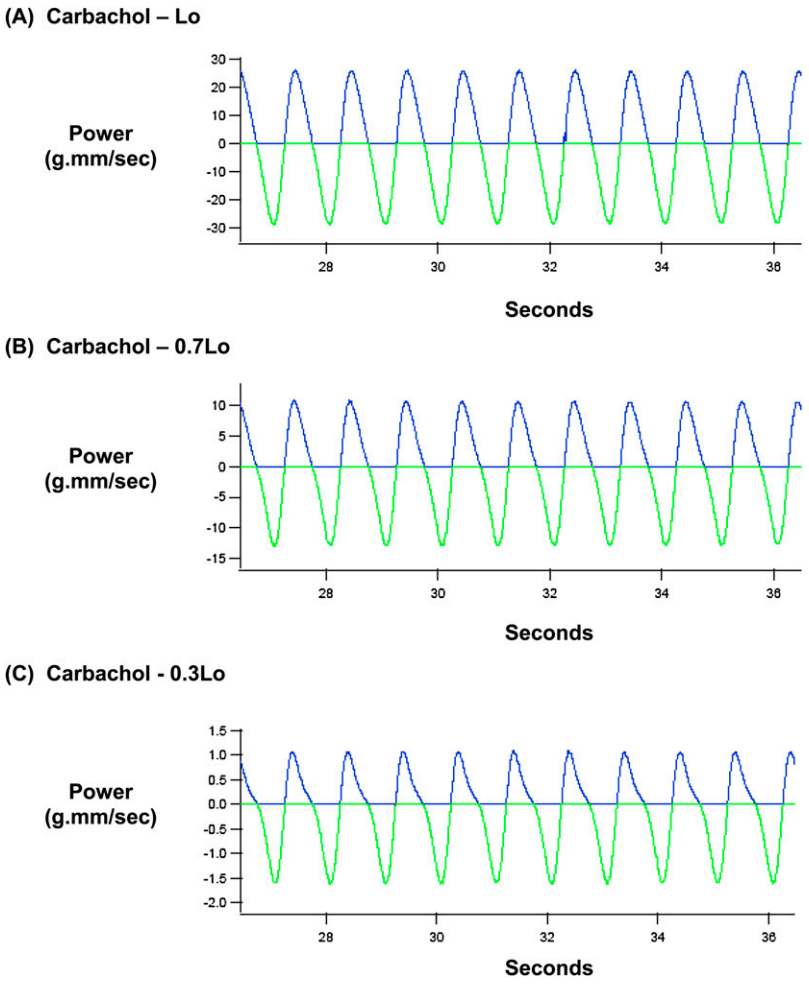

Figure 4. Mechanical power input (*green*) and output (*blue*) during sinusoidal length oscillation of a carbachol-stimulated bovine tracheal smooth muscle held at (*A*) Lo, (*B*) 0.7 Lo, and (*C*) 0.3 Lo. In this experiment, oscillatory amplitude and frequency were 1% Lo and 1 Hz, respectively.

smooth muscle contraction, including phosphatidylinositol breakdown, intracellular [Ca^{2+}] regulation, myosin light chain phosphorylation, paxillin phosphorylation, and focal adhesion kinase phosphorylation (2, 3, 5, 6). In general, all of these signaling pathways are down-regulated at short muscle lengths, and up-regulated at long muscle lengths. Unexpectedly, we found that the cholinergic receptor–mediated cytoskeletal recruitment of actin-binding and integrin-binding proteins exhibited an inverse dependence on muscle length in airway smooth muscle. To our knowledge, this is the first report of length-dependent cytoskeletal remodeling in intact airway smooth muscle.

We found that the cytoskeletal recruitment of Arp3, metavinculin, and talin is stimulated by 1 μM carbachol and modulated by muscle length, whereas the cytoskeletal recruitment of α-actinin and vinculin is stimulated by 1 μM carbachol but not modulated by muscle length. In contrast, neither 1 μM carbachol nor muscle length had a significant effect on the pellet/supernatant ratio of α-SM actin. The finding for α-SM actin was discordant with our previous finding that, at Lo, carbachol stimulated the cytoskeletal recruitment of α-SM actin at 1, 10, and 100 μM (12). The present finding for α-actinin was in general agreement with our previous findings (12). However, the finding for talin was discordant with our previous finding that, at Lo, carbachol stimulated the cytoskeletal recruitment of talin at 1, 10, and 100 μM. A possible explanation for these inconsistencies states that 1 μM is the threshold concentration for the carbachol-stimulated cytoskeletal recruitment of α-SM actin and talin, so that cellular responses at 1 μM carbachol tend to exhibit high variability. Arp3 is a component of the Arp2/3 complex that initiates the branching of actin filaments (14). Metavinculin and talin are linker proteins that connect the intracellular actin cytoskeleton to integrin receptors (1). Therefore, the observed inverse length dependence of the cytoskeletal recruitment of Arp3, metavinculin, and talin suggest that the actin cytoskeleton–integrin complex becomes enriched in cross-linked and branched actin filaments in highly shortened airway smooth muscle cells. This observation was unexpected, but appeared to be consistent with the known effects of mechanical strain on signaling pathways that regulate cytoskeletal remodeling. For example, cholinergic stimulation induces the breakdown of phosphatidylinositol 4,5 bisphosphate (PIP_2) in airway smooth muscle, resulting in the formation of two intracellular messengers (inositol triphosphate and diacylacylglycerol), accompanied by a decrease in the cell membrane content of PIP_2 (32). PIP_2 is known to activate the binding of vinculin to talin and actin, the binding of talin to integrin, and the activation of cell division control protein 42 (Cdc42) and neuronal Wiskott-Aldrich Syndrome protein (N-WASP) for Arp2/3-dependent actin polymerization (22, 23, 33). The cholinergic receptor–mediated breakdown of phosphatidylinositol is length-dependent in airway smooth muscle (2), suggesting that membrane PIP_2 content in cholinergically activated airway smooth muscle cells is up-regulated in short muscle lengths, relative to long muscle lengths. Therefore, the anticipated inverse length dependence of membrane PIP_2 content in cholinergically activated airway smooth muscle cells is one mechanism that may explain the inverse length dependence of the cytoskeletal recruitment of

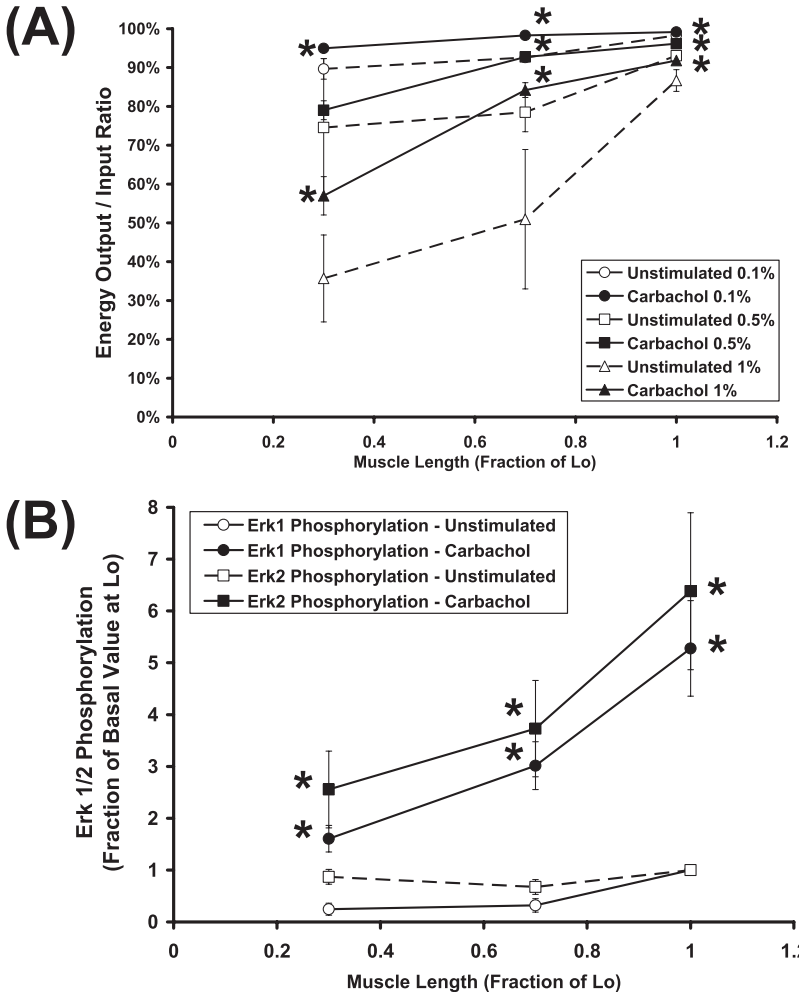

Figure 5. (*A*) Length dependencies of mechanical energy output/input ratios during sinusoidal length oscillation of unstimulated (*open symbols*) and carbachol-stimulated (*solid symbols*) muscle strips. In these experiments, the oscillatory frequency was 1 Hz, and the oscillatory amplitude was 0.1% Lo (*circles*), 0.5% Lo (*squares*), or 1% Lo (triangles). Mechanical energy input and output were calculated by integrating mechanical power input and output, respectively, with time during 10 cycles of length oscillation. Data are presented as means ± SEM (n = 3–7). *Significantly different from basal energy output/input ratio in unstimulated tissues held at the same muscle length ($P < 0.05$). (*B*) Length dependencies of extracellular signal-regulated kinase-1 (Erk1) phosphorylation (*circles*) and Erk2 phosphorylation (*squares*) in unstimulated (*open symbols*) and carbachol-stimulated (*solid symbols*) muscle strips. Labeling with anti-Erk1/2 antibody confirmed that the same amounts of Erk1 and Erk2 were loaded onto individual lanes (data not shown). Therefore, values of phospho-Erk1 and phospho-Erk2 reflect levels of Erk1/2 phosphorylation. In each experiment, the six samples derived from unstimulated and carbachol-stimulated muscle strips held at 0.3, 0.7, or 1.0 Lo were analyzed together by Western blotting. Concentrations of phospho-Erk1 or phospho-Erk2 in each sample were then normalized by the corresponding phospho-Erk1 and phospho-Erk2 concentrations in unstimulated muscle strips held at Lo, shown here as 1. *Significantly different from basal phosphorylation in unstimulated tissues held at the same muscle length. Data are presented as means ± SEM (n = 9).

talin and Arp3. An alternative mechanism involves the length-dependent modulation of the tyrosine phosphorylation of paxillin and focal adhesion kinase in cholinergic receptor–stimulated airway smooth muscle (6). Tyrosine-phosphorylated paxillin was shown to enhance the disassembly of focal adhesions in migrating cells (34). Similarly, the activation of focal adhesion kinase (FAK) was shown to promote cytoskeletal fluidity in fibroblasts (35). Therefore, the length-dependent tyrosine phosphorylation of paxillin and focal adhesion kinase is another mechanism that may explain the inverse dependence of cholinergic receptor–mediated cytoskeletal recruitment in airway smooth muscle.

We studied the mechanical energetics of airway smooth muscle as a function of muscle length by analyzing mechanical energy output/input ratios during sinusoidal length oscillation. This is a novel approach for studying airway smooth muscle mechanics, because it does not require assumptions on force–velocity relations or strain-dependent crossbridge cycling rates, as is necessary in other approaches (36, 37). Furthermore, this approach considers airway smooth muscle as a responder to external mechanical energy inputs, without assuming limits on mechanical energy outputs by airway smooth muscle cells. The analysis of energy output/input during sinusoidal length oscillation is similar to the concept of rebound resilience in mechanical engineering and the physiology of insect flight. In engineering with rubber, rebound resilience is defined as the ratio of energy release after unloading/energy absorption during loading (38). The rebound resilience of rubber is always below 100%, because rubber is only capable of releasing stored energy. In contrast, energy released by asynchronous flight muscles during unloading can be greater than the energy stored during loading because of a stretch-induced delayed activation of muscle contraction, which produces "new" mechanical energy during the unloading phase (39). This mechanism enables asynchronous flight muscles to oscillate wings at high frequency during insect flight, in resonance with the oscillation of the external load imposed by the thorax.

In this study, we used an analysis of energy output/input ratios to integrate the effects of crossbridge cycling and cytoskeletal recruitment on the oscillatory mechanics of airway smooth muscle as a function of muscle length and cholinergic stimulation. We selected frequencies and amplitudes of length oscillation within physiologic range, but sufficient to disrupt crossbridge cycling, and to reveal the contribution of non–crossbridge mechanisms. The oscillatory frequency of 1 Hz is higher than the crossbridge cycling rate (40), but is physiologically attainable in cows during programmed exercise (41). The oscillatory amplitude of 0.1–1% is within the physiologic range of airway deformation during normal breathing (42). Using this approach, we found that the mechanical energy output/input ratio was higher in cholinergically activated than unstimulated airway smooth muscle at all imposed oscillatory amplitudes (0.1%, 0.5%, and 1% Lo) and muscle lengths (0.3, 0.7, and 1.0 Lo; Figure 5A). The enhancing effect of cholinergic stimulation on the mechanical energy output/input ratio at Lo is not surprising, because it can be explained by the relatively high

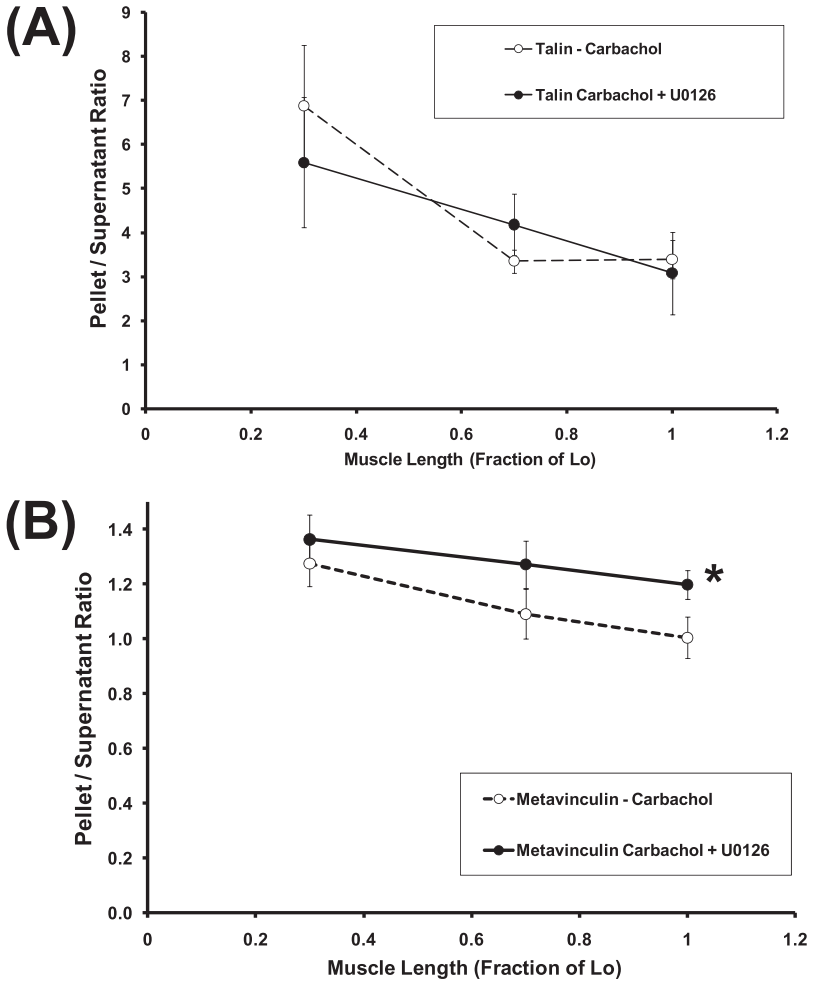

Figure 6. Effects of U0126 on length dependencies of (*A*) pellet/supernatant ratios of talin, and (*B*) pellet/supernatant ratios of metavinculin in carbachol-stimulated muscle strips. *Open* and *solid symbols* represent pellet/supernatant ratios in untreated and U0126-treated tissues, respectively. Data are presented as means ± SEM (n = 8–9). *Significantly different between U0126-treated and untreated values in tissues held at the same muscle length.

level of crossbridge activation at Lo (Table 1). However, the enhancing effect of cholinergic stimulation on the mechanical energy output/input ratio at 0.3 Lo was unexpected, and cannot be explained by crossbridge activation, because cholinergic stimulation did not significantly increase force development at 0.3 Lo. Instead, the observed up-regulation of cytoskeletal recruitment in a highly shortened airway smooth muscle suggests that the cholinergic receptor–mediated strengthening of a force-bearing cytoskeleton (Figures 1 and 2) may explain the enhancing effect of cholinergic stimulation on mechanical output/input ratios in highly shortened airway smooth muscle.

The results of this study indicate a significant length dependence of Erk1/2 activation in 1 μM carbachol-stimulated tissues (Figure 5B). Therefore, we tested the hypothesis that length-dependent Erk1/2 MAPK activation mediates length-dependent cytoskeletal recruitment of talin and metavinculin in 1 μM carbachol-stimulated tissues, using U0126, an inhibitor of Erk1/2 MAPK kinase (MEK1/2). We focused on talin and metavinculin, because muscle length significantly modulates the cytoskeletal recruitment of these two proteins (Figure 2). We found that the inhibition of Erk1/2 MAPK by U0126 significantly altered the cytoskeletal recruitment of metavinculin, but not talin (Figure 6). U0126 did not significantly affect active force development during isometric contractions (Table 1) or mechanical energy output/input ratios during sinusoidal length oscillation (data not shown). Therefore, these results suggest that Erk1/2 MAPK is involved in the length-dependent modulation of the cholinergic receptor–mediated cytoskeletal recruitment of metavinculin, but Erk1/2 MAPK alone is insufficient to explain the length dependence of mechanical energetics in airway smooth muscle. Because Erk1/2 MAPK is one signaling pathway within a complex network of multiple interconnecting signaling pathways that regulate the cytoskeleton–matrix interface in cells (43), Erk1/2 MAPK may differentially regulate the cytoskeletal recruitment of different proteins, depending on the position of the protein in the network.

Based on the observation that cytoskeletal recruitment becomes up-regulated and crossbridge attachment becomes down-regulated at short muscle lengths, and vice versa at long muscle lengths, together with the data on mechanical energetics, we postulate that airway smooth muscle functions as a hybrid biomaterial, capable of switching between operating as a cytoskeleton-based mechanical energy store at short muscle lengths to operating as an actomyosin-powered mechanical energy generator at long muscle lengths (Figure 7). This model is innovative and significant in challenging the current paradigm on cytoskeletal remodeling and tissue mechanics in airway smooth muscle (i.e., that cytoskeletal recruitment and crossbridge force generation occur in parallel) by proposing the alternative hypothesis that the two processes can be dissociated, depending on the mechanical strain. This model holds the potential clinical implication that inhibitors of smooth muscle contractions may not be effective in dilating collapsed airways. Brown and colleagues (44) reported that airway distensiblility, as measured by the forced oscillation technique, was reduced in adults with asthma compared with healthy adults, but was unchanged after bronchodilator administration. The results of our study suggest that the up-regulation

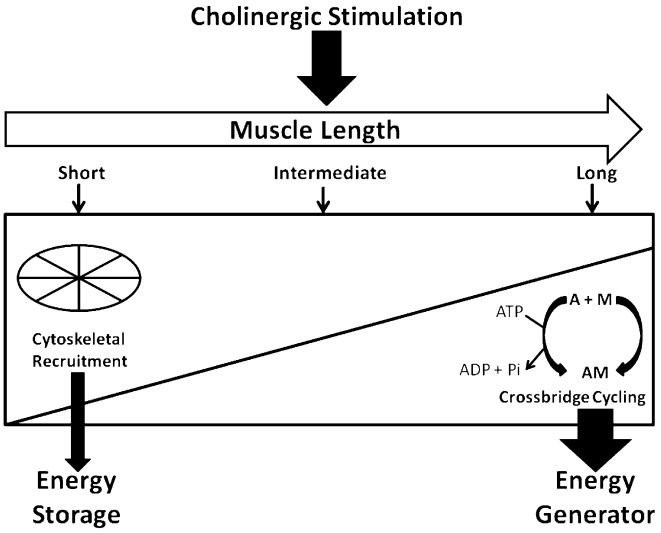

Figure 7. Model of length-dependent modulation of mechanical energetics in cholinergically stimulated airway smooth muscle. This model postulates that airway smooth muscle cell functions as a hybrid biomaterial, capable of switching between operating mostly as a cytoskeleton-based mechanical energy store at short muscle lengths, to operating mostly as an actomyosin-based mechanical energy generator at long muscle lengths. Accordingly, at short muscle lengths, cytoskeletal elasticity enables the recoil of airway smooth muscle against external load. At long muscle lengths, ATP-dependent crossbridge cycling enables the shortening of airway smooth muscle against external load. This model holds the potential clinical implication that inhibitors of smooth muscle contraction may not be effective in dilating collapsed airways. A, actin; M, myosin; AM, actomyosin; ADP, adenosine diphosphate; Pi, inorganic phosphate.

of cytoskeletal recruitment in highly shortened airway smooth muscle may be an important mechanism of reduced airway distensibility in asthma. Accordingly, targeting the signaling molecules involved in cytoskeletal recruitment, such as PIP_2 and focal adhesion kinase, may offer a novel approach to the treatment of obstructive airway diseases such as asthma.

Author Disclosure: T.J.R. received a sponsored grant from the National Institutes of Health for more than $100,001. H.R.K. does not have a financial relationship with a commercial entity that has an interest in the subject of this manuscript. K.L. does not have a financial relationship with a commercial entity that has an interest in the subject of this manuscript. C.-M.H. does not have a financial relationship with a commercial entity that has an interest in the subject of this manuscript.

References

1. Gunst SJ, Zhang W. Actin cytoskeletal dynamics in smooth muscle: a new paradigm for the regulation of smooth muscle contraction. *Am J Physiol Cell Physiol* 2008;295:C576–C587.
2. An SS, Hai CM. Mechanical strain modulates maximal phosphatidylinositol turnover in airway smooth muscle. *Am J Physiol Lung Cell Mol Physiol* 1999;277:L968–L974.
3. An SS, Hai CM. Mechanical signals and mechanosensitive modulation of intracellular [Ca^{2+}] in smooth muscle. *Am J Physiol Cell Physiol* 2000;279:C1375–C1384.
4. Hai CM. Mechanosensitive modulation of receptor-mediated crossbridge activation and cytoskeletal reorganization in airway smooth muscle. *Arch Pharm Res* 2000;23:535–547.
5. Mehta D, Wu MF, Gunst SJ. Role of contractile protein activation in the length-dependent modulation of tracheal smooth muscle force. *Am J Physiol Cell Physiol* 1996;270:C243–C252.
6. Tang D, Mehta D, Gunst SJ. Mechanosensitive tyrosine phosphorylation of paxillin and focal adhesion kinase in tracheal smooth muscle. *Am J Physiol* 1999;276:C250–C258.
7. Youn T, Kim SA, Hai CM. Length-dependent modulation of smooth muscle activation: effects of agonist, cytochalasin, and temperature. *Am J Physiol Cell Physiol* 1998;274:C1601–C1607.
8. Di Paolo G, De Camilli P. Phosphoinositides in cell regulation and membrane dynamics. *Nature* 2006;443:651–657.
9. Fincham VJ, James M, Frame MC, Winder SJ. Active ERK/MAP kinase is targeted to newly forming cell-matrix adhesions by integrin engagement and v-Src. *EMBO J* 2000;19:2911–2923.
10. Webb DJ, Donais K, Whitmore LA, Thomas SM, Turner CE, Parsons JT, Horwitz AF. FAK-Src signaling through paxillin, ERK and MLCK regulates adhesion disassembly. *Nat Cell Biol* 2004;6:154–164.
11. Yin HL, Janmey PA. Phosphoinositide regulation of the actin cytoskeleton. *Annu Rev Physiol* 2003;65:761–789.
12. Kim HR, Hoque M, Hai CM. Cholinergic receptor–mediated differential cytoskeletal recruitment of actin- and integrin-binding proteins in intact airway smooth muscle. *Am J Physiol Cell Physiol* 2004;287:C1375–C1383.
13. Gu Z, Kordowska J, Williams GL, Wang CLA, Hai CM. Erk1/2 MAPK and caldesmon differentially regulate podosome dynamics in A7R5 vascular smooth muscle cells. *Exp Cell Res* 2007;313:849–866.
14. Goley ED, Welch MD. The ARP2/3 complex: an actin nucleator comes of age. *Nat Rev Mol Cell Biol* 2006;7:713–726.
15. Byrne BJ, Kaczorowski YJ, Coutu MD, Craig SW. Chicken vinculin and meta-vinculin are derived from a single gene by alternative splicing of a 207–base pair exon unique to meta-vinculin. *J Biol Chem* 1992;267:12845–12850.
16. Gimona M, Small JV, Moeremans M, Van Damme J, Puype M, Vandekerckhove J. Porcine vinculin and metavinculin differ by a 68-residue insert located close to the carboxy-terminal part of the molecule. *EMBO J* 1988;7:2329–2334.
17. Belkin AM, Ornatsky OI, Kabakov AE, Glukhova MA, Koteliansky VE. Immunolocalization of meta-vinculin in human smooth muscle and cardiac muscles. *J Biol Chem* 1988;263:6631–6635.
18. Goldberg M, Zhang HL, Steinberg SF. Hypoxia alters the subcellular distribution of protein kinase C isoforms in neonatal rat ventricular myocytes. *J Clin Invest* 1997;99:55–61.
19. Harrington EO, Brunelle JL, Shannon CJ, Kim ES, Mennella K, Rounds S. Role of protein kinase C isoforms in rat epididymal microvascular endothelial barrier function. *Am J Respir Cell Mol Biol* 2003;28:626–636.
20. Katoh K, Kano Y, Masuda M, Onishi H, Fujiwara K. Isolation and contraction of the stress fiber. *Mol Biol Cell* 1998;9:1919–1938.
21. Tsutsumi T, Ushiro H, Kosaka T, Kayahara T, Nakano K. Proline- and alanine-rich Ste20-related kinase associates with F-actin and translocates from the cytosol to cytoskeleton upon cellular stresses. *J Biol Chem* 2000;275:9157–9162.
22. Gilmore AP, Burridge K. Regulation of vinculin binding to talin and actin by phosphatidylinositol-4–5-bisphosphate. *Nature* 1996;381:531–535.
23. Martel V, Racaud-Sultan C, Dupe S, Marie C, Paulhe F, Galmiche A, Block MR, Albiges-Rizo C. Conformation, localization, and integrin binding of talin depend on its interaction with phosphoinositides. *J Biol Chem* 2001;276:21217–21227.
24. Tseng S, Kim R, Kim T, Morgan KG, Hai CM. F-actin disruption attenuates agonist-induced [Ca^{2+}], myosin phosphorylation, and force in smooth muscle. *Am J Physiol Cell Physiol* 1997;272:C1960–C1967.
25. Kanefsky J, Lenburg M, Hai CM. Cholinergic receptor and cyclic stretch-mediated inflammatory gene expression in intact ASM. *Am J Respir Cell Mol Biol* 2006;34:417–425.
26. Kawai M, Halvorson HR. Force transients and minimum cross-bridge models in muscular contraction. *J Muscle Res Cell Motil* 2007;28:371–395.
27. Walsh MP. Smooth muscle caldesmon. *Prog Clin Biol Res* 1990;245:127–140.
28. Franco SJ, Huttenlocher A. Regulating cell migration: calpains make the cut. *J Cell Sci* 2005;118:3829–3838.
29. Roberts GCK, Critchley DR. Structural and biophysical properties of the integrin-associated cytoskeletal protein talin. *Biophysical Reviews* 2009;1:61–69.
30. Tranqui L, Block MR. Intracellular processing of talin occurs within focal adhesions. *Exp Cell Res* 1995;217:149–156.
31. Oostveen E, MacLeod D, Lorino H, Farre R, Hantos Z, Desager K, Marchal F. The forced oscillation technique in clinical practice: methodology, recommendations and future developments. *Eur Respir J* 2003;22:1026–1041.

32. Chilvers ER, Batty IH, Challiss RAJ, Barnes PJ, Nahorski SR. Determination of mass changes in phosphatidylinositol 4,5-bisphosphate and evidence for agonist-stimulated metabolism of inositol 1,4,5-trisphosphate in airway smooth muscle. *Biochem J* 1991;275:373–379.
33. Rohatgi R, Ho HYH, Kirschner MW. Mechanism of N-WASP activation by CDC42 and phosphatidylinositol 4,5-bisphosphate. *J Cell Biol* 2000;150:1299–1309.
34. Deakin NO, Turner CE. Paxillin comes of age. *J Cell Sci* 2008;121:2435–2444.
35. Mitra SK, Hanson DA, Schlaepfer DD. Focal adhesion kinase: in command and control of cell motility. *Nat Rev Mol Cell Biol* 2005;6:56–68.
36. Bates JHT, Lauzon AM. Modeling the oscillation dynamics of activated airway smooth muscle strips. *Am J Physiol Lung Cell Mol Physiol* 2005;289:L849–L855.
37. Mijailovich SM, Butler JP, Fredberg JJ. Perturbed equilibria of myosin binding in airway smooth muscle: bond-length distributions, mechanics, and ATP metabolism. *Biophys J* 2000;79:2667–2681.
38. Treloar LRG. Physics of rubber elasticity, 3rd edition. London: Oxford University Press; 2009. pp. 15–16.
39. Josephson RK, Malamud JG, Stokes DR. Asynchronous muscle: a primer. *J Exp Biol* 2000;203:2713–2722.
40. Du Y, Al-Jumaily AM, Shukla H. Smooth muscle stiffness variation due to external longitudinal oscillations. *J Biomech* 2007;40:3207–3214.
41. Blake JT, Olsen JD, Walters JL, Lamb RC. Attaining and measuring physical fitness in dairy cattle. *J Dairy Sci* 1982;65:1544–1555.
42. Fredberg JJ, Inouye D, Miller B, Nathan M, Jafari S, Raboudi SH, Butler JP, Shore SA. Airway smooth muscle, tidal stretches, and dynamically determined contractile states. *Am J Respir Crit Care Med* 1997;156:1752–1759.
43. Zamir E, Geiger B. Molecular complexity and dynamics of cell-matrix adhesions. *J Cell Sci* 2001;114:3583–3590.
44. Brown NJ, Salome CM, Berend N, Thorpe CW, King GC. Airway distensibility in adults with asthma and healthy adults, measured by forced oscillation technique. *Am J Respir Crit Care Med* 2007;176:129–137.